Eur. Phys. J. C (2005)
Digital Object Identifier (DOI) 10.1140/epjc/s2005-02218-9

THE EUROPEAN PHYSICAL JOURNAL C

# Charm production in the STAR experiment at RHIC

A.A.P. Suaide[a] on behalf of the STAR Collaboration

J. Adams[3], M.M. Aggarwal[29], Z. Ahammed[43], J. Amonett[20], B.D. Anderson[20], D. Arkhipkin[13], G.S. Averichev[12], S.K. Badyal[19], Y. Bai[27], J. Balewski[17], O. Barannikova[32], L.S. Barnby[3], J. Baudot[18], S. Bekele[28], V.V. Belaga[12], A. Bellingeri-Laurikainen[38], R. Bellwied[46], J. Berger[14], B.I. Bezverkhny[48], S. Bharadwaj[33], A. Bhasin[19], A.K. Bhati[29], V.S. Bhatia[29], H. Bichsel[45], J. Bielcik[48], J. Bielcikova[48], A. Billmeier[46], L.C. Bland[4], C.O. Blyth[3], S. Blyth[21], B.E. Bonner[34], M. Botje[27], A. Boucham[38], J. Bouchet[38], A.V. Brandin[25], A. Bravar[4], M. Bystersky[11], R.V. Cadman[1], X.Z. Cai[37], H. Caines[48], M. Calderón de la Barca Sánchez[17], J. Castillo[21], O. Catu[48], D. Cebra[7], Z. Chajecki[28], P. Chaloupka[11], S. Chattopadhyay[43], H.F. Chen[36], Y. Chen[8], J. Cheng[41], M. Cherney[10], A. Chikanian[48], W. Christie[4], J.P. Coffin[18], T.M. Cormier[46], M.R. Cosentino[35], J.G. Cramer[45], H.J. Crawford[6], D. Das[43], S. Das[43], M. Daugherity[40], M.M. de Moura[35], T.G. Dedovich[12], A.A. Derevschikov[31], L. Didenko[4], T. Dietel[14], S.M. Dogra[19], W.J. Dong[8], X. Dong[36], J.E. Draper[7], F. Du[48], A.K. Dubey[15], V.B. Dunin[12], J.C. Dunlop[4], M.R. Dutta Mazumdar[43], V. Eckardt[23], W.R. Edwards[21], L.G. Efimov[12], V. Emelianov[25], J. Engelage[6], G. Eppley[34], B. Erazmus[38], M. Estienne[38], P. Fachini[4], J. Faivre[18], R. Fatemi[17], J. Fedorisin[12], K. Filimonov[21], P. Filip[11], E. Finch[48], V. Fine[4], Y. Fisyak[4], K.S.F. Fornazier[35], J. Fu[41], C.A. Gagliardi[39], L. Gaillard[3], J. Gans[48], M.S. Ganti[43], F. Geurts[34], V. Ghazikhanian[8], P. Ghosh[43], J.E. Gonzalez[8], H. Gos[44], O. Grachov[46], O. Grebenyuk[27], D. Grosnick[42], S.M. Guertin[8], Y. Guo[46], A. Gupta[19], T.D. Gutierrez[7], T.J. Hallman[4], A. Hamed[46], D. Hardtke[21], J.W. Harris[48], M. Heinz[2], T.W. Henry[39], S. Hepplemann[30], B. Hippolyte[18], A. Hirsch[32], E. Hjort[21], G.W. Hoffmann[40], M. Horner[21], H.Z. Huang[8], S.L. Huang[36], E.W. Hughes[5], T.J. Humanic[28], G. Igo[8], A. Ishihara[40], P. Jacobs[21], W.W. Jacobs[17], M Jedynak[44], H. Jiang[8], P.G. Jones[3], E.G. Judd[6], S. Kabana[2], K. Kang[41], M. Kaplan[9], D. Keane[20], A. Kechechyan[12], V.Yu. Khodyrev[31], J. Kiryluk[22], A. Kisiel[44], E.M. Kislov[12], J. Klay[21], S.R. Klein[21], D.D. Koetke[42], T. Kollegger[14], M. Kopytine[20], L. Kotchenda[25], K.L. Kowalik[21], M. Kramer[26], P. Kravtsov[25], V.I. Kravtsov[31], K. Krueger[1], C. Kuhn[18], A.I. Kulikov[12], A. Kumar[29], R.Kh. Kutuev[13], A.A. Kuznetsov[12], M.A.C. Lamont[48], J.M. Landgraf[4], S. Lange[14], F. Laue[4], J. Lauret[4], A. Lebedev[4], R. Lednicky[12], S. Lehocka[12], M.J. LeVine[4], C. Li[36], Q. Li[46], Y. Li[41], G. Lin[48], S.J. Lindenbaum[26], M.A. Lisa[28], F. Liu[47], H. Liu[36], J. Liu[34], L. Liu[47], Q.J. Liu[45], Z. Liu[47], T. Ljubicic[4], W.J. Llope[34], H. Long[8], R.S. Longacre[4], M. Lopez-Noriega[28], W.A. Love[4], Y. Lu[47], T. Ludlam[4], D. Lynn[4], G.L. Ma[37], J.G. Ma[8], Y.G. Ma[37], D. Magestro[28], S. Mahajan[19], D.P. Mahapatra[15], R. Majka[48], L.K. Mangotra[19], R. Manweiler[42], S. Margetis[20], C. Markert[20], L. Martin[38], J.N. Marx[21], H.S. Matis[21], Yu.A. Matulenko[31], C.J. McClain[1], T.S. McShane[10], F. Meissner[21], Yu. Melnick[31], A. Meschanin[31], M.L. Miller[22], N.G. Minaev[31], C. Mironov[20], A. Mischke[27], D.K. Mishra[15], J. Mitchell[34], B. Mohanty[43], L. Molnar[32], C.F. Moore[40], D.A. Morozov[31], M.G. Munhoz[35], B.K. Nandi[43], S.K. Nayak[19], T.K. Nayak[43], J.M. Nelson[3], P.K. Netrakanti[43], V.A. Nikitin[13], L.V. Nogach[31], S.B. Nurushev[31], G. Odyniec[21], A. Ogawa[4], V. Okorokov[25], M. Oldenburg[21], D. Olson[21], S.K. Pal[43], Y. Panebratsev[12], S.Y. Panitkin[4], A.I. Pavlinov[46], T. Pawlak[44], T. Peitzmann[27], V. Perevoztchikov[4], C. Perkins[6], W. Peryt[44], V.A. Petrov[46], S.C. Phatak[15], R. Picha[7], M. Planinic[49], J. Pluta[44], N. Porile[32], J. Porter[45], A.M. Poskanzer[21], M. Potekhin[4], E. Potrebenikova[12], B.V.K.S. Potukuchi[19], D. Prindle[45], C. Pruneau[46], J. Putschke[21], G. Rakness[30], R. Raniwala[33], S. Raniwala[33], O. Ravel[38], R.L. Ray[40], S.V. Razin[12], D. Reichhold[32], J.G. Reid[45], J. Reinnarth[38], G. Renault[38], F. Retiere[21], A. Ridiger[25], H.G. Ritter[21], J.B. Roberts[34], O.V. Rogachevskiy[12], J.L. Romero[7], A. Rose[21], C. Roy[38], L. Ruan[36], M.J. Russcher[27], R. Sahoo[15], I. Sakrejda[21], S. Salur[48], J. Sandweiss[48], M. Sarsour[17], I. Savin[13], P.S. Sazhin[12], J. Schambach[40], R.P. Scharenberg[32], N. Schmitz[23], K. Schweda[21], J. Seger[10], P. Seyboth[23], E. Shahaliev[12], M. Shao[36], W. Shao[5], M. Sharma[29], W.Q. Shen[37], K.E. Shestermanov[31], S.S. Shimanskiy[12], E Sichtermann[21], F. Simon[23], R.N. Singaraju[43], N. Smirnov[48], R. Snellings[27], G. Sood[42], P. Sorensen[21], J. Sowinski[17], J. Speltz[18], H.M. Spinka[1], B. Srivastava[32], A. Stadnik[12], T.D.S. Stanislaus[42], R. Stock[14], A. Stolpovsky[46], M. Strikhanov[25], B. Stringfellow[32], A.A.P. Suaide[35], E. Sugarbaker[28], C. Suire[4], M. Sumbera[11], B. Surrow[22], M. Swanger[10], T.J.M. Symons[21], A. Szanto de Toledo[35], A. Tai[8], J. Takahashi[35], A.H. Tang[27], T. Tarnowsky[32], D. Thein[8], J.H. Thomas[21], S. Timoshenko[25], M. Tokarev[12], T.A. Trainor[45], S. Trentalange[8], R.E. Tribble[39], O.D. Tsai[8], J. Ulery[32], T. Ullrich[4], D.G. Underwood[1], G. Van Buren[4], M. van Leeuwen[21], A.M. Vander Molen[24], R. Varma[16], I.M. Vasilevski[13], A.N. Vasiliev[31], R. Vernet[18], S.E. Vigdor[17], Y.P. Viyogi[43], S. Vokal[12], S.A. Voloshin[46], W.T. Waggoner[10], F. Wang[32], G. Wang[20], G. Wang[5], X.L. Wang[36], Y. Wang[40], Y. Wang[41], Z.M. Wang[36], H. Ward[40], J.W. Watson[20], J.C. Webb[17], G.D. Westfall[24], A. Wetzler[21], C. Whitten Jr.[8], H. Wieman[21], S.W. Wissink[17], R. Witt[2], J. Wood[8], J. Wu[36], N. Xu[21], Z. Xu[4],

[a] e-mail: suaide@if.usp.br

Z.Z. Xu[36], E. Yamamoto[21], P. Yepes[34], V.I. Yurevich[12], I. Zborovsky[11], H. Zhang[4], W.M. Zhang[20], Y. Zhang[36], Z.P. Zhang[36], R. Zoulkarneev[13], Y. Zoulkarneeva[13], A.N. Zubarev[12]

[1] Argonne National Laboratory, Argonne, Illinois 60439, USA
[2] University of Bern, 3012 Bern, Switzerland
[3] University of Birmingham, Birmingham, UK
[4] Brookhaven National Laboratory, Upton, New York 11973, USA
[5] California Institute of Technology, Pasadena, California 91125, USA
[6] University of California, Berkeley, California 94720, USA
[7] University of California, Davis, California 95616, USA
[8] University of California, Los Angeles, California 90095, USA
[9] Carnegie Mellon University, Pittsburgh, Pennsylvania 15213
[10] Creighton University, Omaha, Nebraska 68178
[11] Nuclear Physics Institute AS CR, 250 68 Řež/Prague, Czech Republic
[12] Laboratory for High Energy (JINR), Dubna, Russia
[13] Particle Physics Laboratory (JINR), Dubna, Russia
[14] University of Frankfurt, Frankfurt, Germany
[15] Institute of Physics, Bhubaneswar 751005, India
[16] Indian Institute of Technology, Mumbai, India
[17] Indiana University, Bloomington, Indiana 47408, USA
[18] Institut de Recherches Subatomiques, Strasbourg, France
[19] University of Jammu, Jammu 180001, India
[20] Kent State University, Kent, Ohio 44242, USA
[21] Lawrence Berkeley National Laboratory, Berkeley, California 94720, USA
[22] Massachusetts Institute of Technology, Cambridge, MA 02139-4307, USA
[23] Max-Planck-Institut für Physik, Munich, Germany
[24] Michigan State University, East Lansing, Michigan 48824, USA
[25] Moscow Engineering Physics Institute, Moscow Russia
[26] City College of New York, New York City, New York 10031, USA
[27] NIKHEF and Utrecht University, Amsterdam, The Netherlands
[28] Ohio State University, Columbus, Ohio 43210, USA
[29] Panjab University, Chandigarh 160014, India
[30] Pennsylvania State University, University Park, Pennsylvania 16802, USA
[31] Institute of High Energy Physics, Protvino, Russia
[32] Purdue University, West Lafayette, Indiana 47907, USA
[33] University of Rajasthan, Jaipur 302004, India
[34] Rice University, Houston, Texas 77251, USA
[35] Universidade de Sao Paulo, Sao Paulo, Brazil
[36] University of Science & Technology of China, Anhui 230027, P.R. China
[37] Shanghai Institute of Applied Physics, Shanghai 201800, P.R. China
[38] SUBATECH, Nantes, France
[39] Texas A&M University, College Station, Texas 77843, USA
[40] University of Texas, Austin, Texas 78712, USA
[41] Tsinghua University, Beijing 100084, P.R. China
[42] Valparaiso University, Valparaiso, Indiana 46383, USA
[43] Variable Energy Cyclotron Centre, Kolkata 700064, India
[44] Warsaw University of Technology, Warsaw, Poland
[45] University of Washington, Seattle, Washington 98195, USA
[46] Wayne State University, Detroit, Michigan 48201, USA
[47] Institute of Particle Physics, CCNU (HZNU), Wuhan 430079, P.R. China
[48] Yale University, New Haven, Connecticut 06520, USA
[49] University of Zagreb, Zagreb, 10002, Croatia

Received: 14 February 2005 /
Published online: 28 June 2005 – 

**Abstract.** The single electron spectrum over a sufficiently broad $p_{\mathrm{T}}$ range provides an indirect measurement of charm and beauty production at RHIC energies. Heavy-quarks are produced in parton-parton scattering in the initial phase of the collision and thus provide important information about the initial configuration of the colliding nuclei. Even more important, the final state spectra reflect the interactions of these heavy partons with the medium and thus allow us to probe the properties of the hot and dense system created in heavy-ion collisions. We present preliminary measurements of electron and positron $p_{\mathrm{T}}$ spectra in pp and

d+Au as well as preliminary elliptic flow measurements in Au+Au collisions at $\sqrt{s_{NN}} = 200$ GeV performed by the STAR experiment. We describe the measurement techniques used to discriminate electrons from hadrons and compare the results with theoretical calculations.

**PACS.** 25.75.-q

## 1 Introduction

The study of heavy-quark hadrons produced in high energy pp collisions is an important tool to further expand our knowledge of the interactions described by Quantum Chromodynamics (QCD). Because of their large masses, their production can be calculated by perturbative QCD (pQCD) [1]. There have been many improvements in the pQCD predictions [2] over the last few years but many uncertainties in the leading order (LO) and next to leading order (NLO) calculations remain. Nevertheless, the experimental results are, in general, in qualitative agreement with the calculations [1,2]. Remaining uncertainties depend mostly on the quark masses, factorization scale, and parton distribution functions (PDF) used in the calculations.

Systematic studies on heavy-quark production in pp and p+A collisions and the detailed comparison with theoretical predictions will provide important information about the parton distribution functions, such as the initial state gluon densities in these systems [3] as well as nuclear effects. In addition, heavy-quark measurements are important to understand the behavior of matter produced in high energy A+A collisions at the Relativistic Heavy-Ion Collider (RHIC). These collisions have opened a new domain in the exploration of strongly interacting matter at high energy densities. High temperatures and densities may be generated in the most central (head-on) nuclear collisions, possibly creating the conditions in which a phase of deconfined quarks and gluons exists [4,5]. The measurements at RHIC and comparison to theoretical calculations suggest that a dense equilibrated system has been indeed generated in the collision and that it expands as an ideal hydrodynamic fluid. The good agreement between hydrodynamic calculations and the measurements of inclusive particle spectra and elliptic flow [6] are consistent with the onset of a hydrodynamic evolution at a time $\tau_0 < 1$ fm/$c$ after the collision [7]. The strong suppression observed for high-$p_{\rm T}$ hadrons [8–10] suggests that the system created is extremely dense and dissipative.

Heavy-quark measurements will improve our knowledge about the matter produced in the collisions at RHIC. In heavy-ion collisions, heavy-quark production rates are expected to be an important diagnostics tool of the quark gluon plasma (QGP). In Au+Au collisions, medium effects such as heavy quark energy loss can be studied by comparing the $p_{\rm T}$ distributions of beauty and charm production with those of light-flavor hadrons. The suppression of small angle gluon radiation for heavy quarks, the so-called dead cone effect, would decrease the amount of energy loss substantially [11], implying that the suppression of heavy quark mesons at high-$p_{\rm T}$ is expected to be smaller than the one observed for lighter hadrons at RHIC [8]. Also of great interest is the study of elliptic flow of heavy-quark mesons. Quark coalescence models imply that the measurement of elliptic flow ($v_2$) of D mesons reflects approximately the flow of $c$ quarks. Due to the large mass of the $c$ quark, Dong *et al.* [12] argue that large $v_{2c}$ values can only be achieved if re-scattering in a partonic phase is strong enough to also thermalize the light quarks. Moreover, measuring open charm and beauty production at RHIC provides essential reference data for studies of color screening via quarkonium suppression [13].

Direct reconstruction of heavy-quark mesons through their respective hadronic decay modes [14] is very difficult to perform in high multiplicity events. However, the measurement of heavy flavor mesons through their semileptonic decay channel provides an efficient alternative even at the highest multiplicities. In this paper we report the current status of heavy-quark measurements in pp, d+Au and Au+Au collisions at $\sqrt{s_{NN}} = 200$ GeV performed by the STAR [15] experiment at RHIC.

## 2 Experimental setup

STAR [15] is a large acceptance experiment composed of many individual detector subsystems, many of them installed inside a large solenoidal magnet of 0.5 Tesla. In the following, we describe the detectors that are relevant to the present analysis.

The Time Projection Chamber (TPC) has a pseudorapidity coverage of $|\eta| \leq 1.8$ for collisions in the center of STAR with full azimuthal coverage. For charged tracks in $|\eta| < 1$, the TPC provides up to 45 independent spatial and specific ionization $\mathrm{d}E/\mathrm{d}x$ measurements. The $\mathrm{d}E/\mathrm{d}x$ measurement, in combination with the momentum determination, determines the particle mass within a limited kinematic region ($p < 1$ GeV/$c$).

Two other detectors play an important role in the electron identification procedure: the Time of Flight system (ToF) [15] and the Barrel Electromagnetic Calorimeter (EMC) [15]. The Time of Flight used in the electron identification is a prototype of the full ToF detector, based on a multi-gap resistive plate chamber. It covers $-1 < \eta < 0$ and $\Delta\phi = 6^\circ$, and allows particle identification for $p_T < 3.5$ GeV/$c$.

The barrel Electromagnetic Calorimeter located just inside the coils of the STAR solenoidal magnet, with a radius relative to the beam line of 2.3 m, is a lead-scintillator sampling electromagnetic calorimeter with equal volumes of lead and scintillator. The electromagnetic energy resolution of the detector is $\delta E/E \sim 0.16/\sqrt{E}$. The results presented in this work use the first EMC patch installed for the 2003 RHIC run, that consisted of 60 modules, half of the full planned detector, with cover-

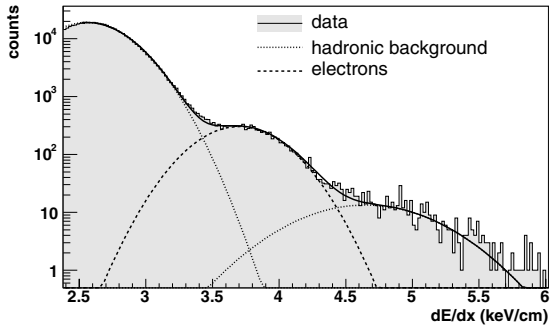


**Fig. 1.** $\mathrm{d}E/\mathrm{d}x$ distribution for particles with $1.5 < p < 8$ GeV/$c$. The lines are Gaussian fits to the spectrum

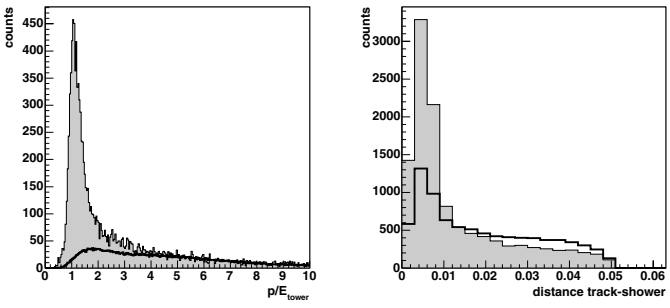


**Fig. 2.** Left: $p/E_{\mathrm{tower}}$ distributions. Right: Distance in the $\eta-\phi$ plane between extrapolated track and SMD shower position. Filled histograms are the distributions for electrons and the non-filled ones are distributions for hadrons

age $0 < \eta < 1$ and $\Delta\phi = 360°$. Each EMC module is composed of 40 towers (20 towers in $\eta$ by 2 towers in $\phi$) projecting to the center of the STAR detector. The tower size is $(\Delta\eta, \Delta\phi) = (0.05, 0.05)$, which, at the radius of the detector's front face, corresponds to a physical size of approximately $10 \times 10$ cm$^2$. The tower depth is 21 radiation lengths ($X_0$), corresponding to a little less than 1 hadronic interaction length. A multi-wire gaseous Shower Max Detector (SMD) is installed at approximately $5X_0$ inside each calorimeter module and allows to measure the electromagnetic shower shape and position with high precision, $(\Delta\eta, \Delta\phi) \sim (0.007, 0.007)$.

## 3 Electron identification in STAR

### 3.1 Electron selection

Electron identification is based on a pre-selection of candidates using $\mathrm{d}E/\mathrm{d}x$ in the TPC. Electrons in the momentum range between 1.5 and 8 GeV/$c$ have slightly higher $\mathrm{d}E/\mathrm{d}x$ values when compared to hadrons (Fig. 1). A $\mathrm{d}E/\mathrm{d}x$ cut in this momentum range provides initial discrimination power on the order of $e/h \sim 500$ with high efficiency.

Electrons can be identified with the ToF system in the low momentum region ($0.2 < p_{\mathrm{T}} < 3$ GeV/$c$) using a combination of velocity ($\beta$) measured in the ToF and $\mathrm{d}E/\mathrm{d}x$ from the TPC. Applying a cut of $|1/\beta - 1| \leq 0.03$ allows us to remove hadrons crossing the electron $\mathrm{d}E/\mathrm{d}x$ band in the low momentum region. The convolution of the TPC tracking efficiency with the ToF hit matching efficiency is on the order of 90 %. The remaining hadron contamination is evaluated to be about 10–15 % of the selected candidates.

High-$p_{\mathrm{T}}$ electrons ($p_T > 1.5$ GeV/$c$) can be identified by combining the TPC and EMC information. Electron candidates selected using the $\mathrm{d}E/\mathrm{d}x$ method are extrapolated to the EMC detector and the energy deposited in the matching tower is compared to their momentum. Electrons show a peak at $p/E_{\mathrm{tower}} \sim 1$ while hadrons have a considerable wider distribution. Figure 2-left depicts the $p/E_{\mathrm{tower}}$ spectrum for the electron candidates exhibiting a well pronounced electron peak. The residual hadronic background is shown as a solid line in the spectrum. After hadronic background subtraction the electron peak is not centered at 1 due to energy leakage to neighbor towers. The amount of leakage depends on the distance to the center of the tower hit by the electron and it is well described by GEANT simulations of the detector response.

The SMD plays an important role in the electron identification procedure. In general, hadronic showers are not well developed compared to electromagnetic showers at SMD depth. The resulting differences are used to enhance the electron discrimination power. The procedure used in this analysis is based on high thresholds in the shower max reconstruction. Electrons will have showers reconstructed well above these cuts while the majority of hadrons will not pass this requirement. We also compare the distance of the extrapolated particle to the reconstructed shower. Because of the poorly developed showers in the case of hadrons, this distance will have a much wider distribution, as seen in Fig. 2-right. The overall electron detection efficiency was obtained by embedding simulated electrons into real events and was found to be $\sim 50$ % and independent of $p_{\mathrm{T}}$ for electrons with $p_{\mathrm{T}} > 2$ GeV/$c$.

Figure 3 depicts the STAR-EMC inclusive electron spectra for d+Au and pp collisions. It also depicts STAR-ToF inclusive electron measurements for the same systems [14]. In both cases, the electron transverse momentum is obtained using the STAR-TPC tracking information. The data is normalized to represent the measurement in one unit of pseudorapidity and full azimuth. EMC and ToF measurements agree very well in the overlap region. The error bars reflect the statistical errors while the boxes represent the systematic uncertainty on the measurements. The main systematic uncertainties are due to the efficiency and acceptance corrections.

### 3.2 Background subtraction

The inclusive electron spectra are composed of contributions from many different sources. We can classify the sources of electrons into two categories: (i) the physics signal of non-photonic electrons (electrons from heavy quark semi-leptonic decays and Drell-Yan); (ii) all other sources,

mostly of photonic origin and misidentified hadrons, which we will refer to as background. There are many sources of background contributing to the inclusive electron yield that need to be removed from the spectra in order to extract the physics signal.

The hadron contamination was estimated by selecting hadrons using TPC $\mathrm{d}E/\mathrm{d}x$ and computing how many of them are identified as electrons in the EMC. Residual hadronic contamination is in the order of 3 % of the inclusive electron for $p_{\mathrm{T}} = 2$ GeV/$c$ and 8 % for $p_{\mathrm{T}} = 6$ GeV/$c$. Photonic electrons come mostly from photon conversion in the detector and $\pi^0$ Dalitz decays (approximately 95 % of all the photonic background). Leptonic and semi-leptonic decays of many other hadrons contribute to the electron background on a much smaller level. Their contribution needs to be estimated through simulations. Most of the photon conversions and $\pi^0$ Dalitz decays can be removed by calculating the squared invariant mass, $m^2$, spectrum of di-electrons. For the background subtraction, the second electron in the pair is selected using only the TPC $\mathrm{d}E/\mathrm{d}x$ information in order to maximize efficiency. Figure 4-left shows the $m^2$ spectrum for opposite and same charge electron pairs. A cut of $m^2 < 0.02$ (GeV/$c^2$)$^2$ removes most of the photon conversion and Dalitz decay electrons. By embedding photons and $\pi^0$ into real events it was found that the efficiency of background recognition and hence subtraction using this technique is fairly constant with the electron $p_{\mathrm{T}}$ at $\sim 65\%$. The remaining background, mainly composed of $\eta$, $\omega$, $\phi$ and $\rho$ decays, was estimated from Pythia [16] and HIJING [17] simulations and it is on the level of a few percent of the total background. Figure 4-right shows the ratio between the physics signal and the background electrons. The overall signal to background ratio improves substantially at high-$p_{\mathrm{T}}$.

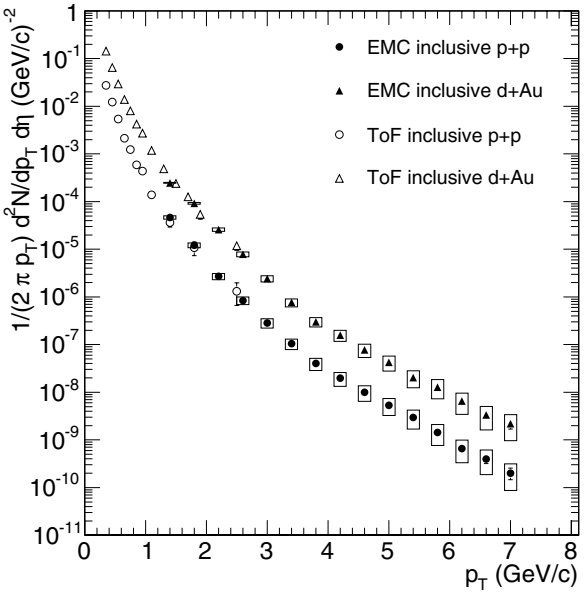


**Fig. 3.** Inclusive electron spectra for d+Au (triangles) and pp (circles) collisions at $\sqrt{s_{NN}} = 200$ GeV. The error bars indicate the statistical errors and the boxes show the systematic uncertainties

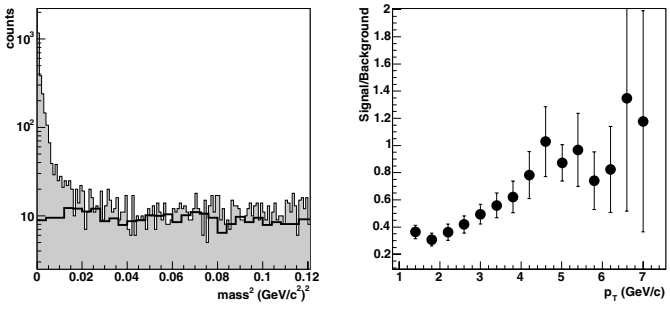


**Fig. 4.** Left: $m^2$ spectra for $e^+e^-$ pairs (histogram) and same charge sign pair (line). Right: Signal to background ratio for electrons as a function of electron $p_{\mathrm{T}}$

## 4 Results and discussion

### 4.1 Non-photonic electron spectra and charm cross section

Figure 5-top shows the non-photonic electron spectra (after background subtraction) for d+Au and pp collisions at $\sqrt{s_{NN}} = 200$ GeV. The pseudorapidity and azimuthal coverage of each measurement matches the detector acceptance (ToF acceptance in the case of ToF+TPC data and EMC acceptance for the EMC+TPC data). Both measurements were normalized to represent the electron production in one unity of pseudorapidity and full azimuthal coverage. The error bars depict statistical errors and the boxes the systematic uncertainties. The main sources of systematic uncertainties are the background subtraction, efficiency and acceptance corrections. The data shown are preliminary and the final assessment of the systematic error, currently $\sim 30\,\%$, is subject to further evaluation.

The lines in the Figure 5-top show the electron spectra prediction for pp collisions from Pythia simulations. The thin solid and dashed lines are predictions for electrons from D and B mesons decays, respectively. The dash-dotted line is the contribution from B mesons decaying into D mesons before decaying to electrons; their contribution to the total yield is negligible. The dotted line shows the contribution from Drell-Yan. The thick solid line is the total electron yield prediction including all the processes mentioned above. The Pythia parameters used in the current simulations are: $\langle K_{\mathrm{T}} \rangle = 2$ GeV/$c$; $m_c = 1.7$ GeV/$c^2$; $K_{\mathrm{factor}} = 2.2$; CTEQ5M1 and PARP(67) = 4 (parton virtuality factor). It is important to notice that the Pythia simulation is not a fit to the data but just a representation of what may be the sources of electrons observed. We note, however, that electrons at moderate to high $p_{\mathrm{T}}$ ($p_{\mathrm{T}} > 3.5$ GeV/$c$) have a significant to dominant contribution from B decays. Figure 5-bottom shows the ratio of the d+Au and pp spectra, $R_{dAu}$, normalized by the number of binary nucleon-nucleon collisions, as a function of $p_{\mathrm{T}}$. The ratio is approximately consistent with unity for the entire momentum range, suggesting that the electron

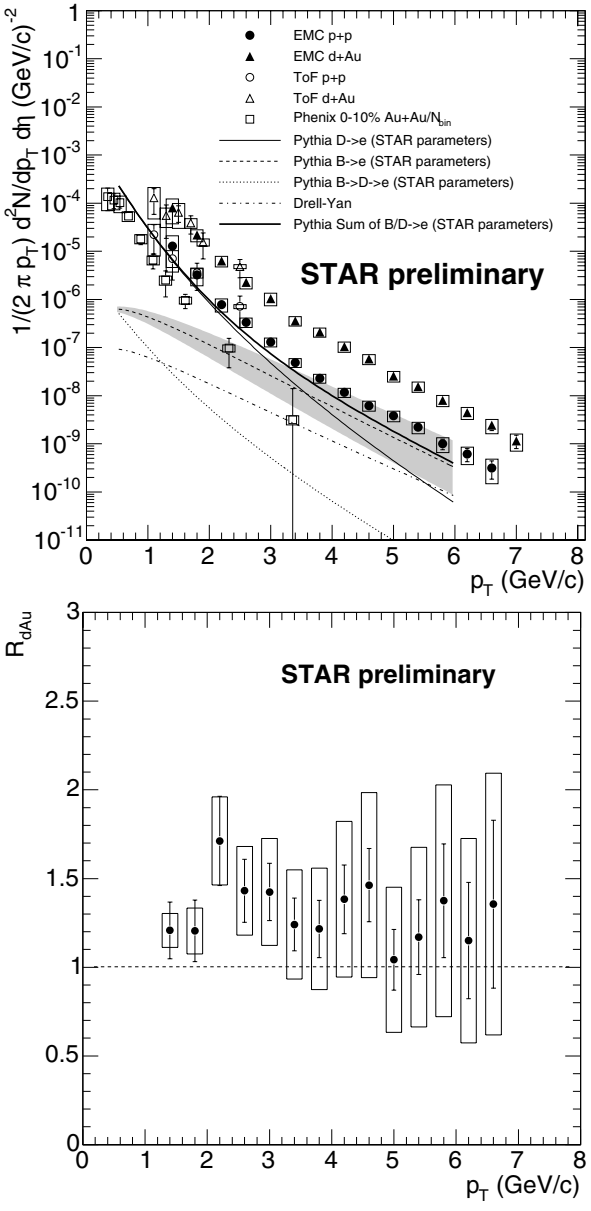


**Fig. 5.** Top: Non-photonic electron spectra for d+Au (triangles) and pp (circles) collisions. The measurements were normalized to represent the electron production in one unity of pseudorapidity and full azimuthal coverage. The error bars indicate the statistical errors and the boxes show the systematic uncertainties. The lines show Pythia simulations (see text for parameters). The square points correspond to the 0–10 % Au+Au electrons from the PHENIX experiment [18], normalized by the number of binary collisions. Bottom: $R_{dAu}$ for electrons at $\sqrt{s_{NN}} = 200$ GeV

production in d+Au collisions follows a simple binary scaling law from pp collisions. However, a small Cronin type enhancement cannot be ruled out.

Figure 5-top also shows the non-photonic spectrum for central 200 GeV Au+Au collisions measured by the PHENIX experiment [18] ($|\eta| < 0.35$ and $\Delta\phi = \pi/4$). Figure 5-top shows a significant difference between the

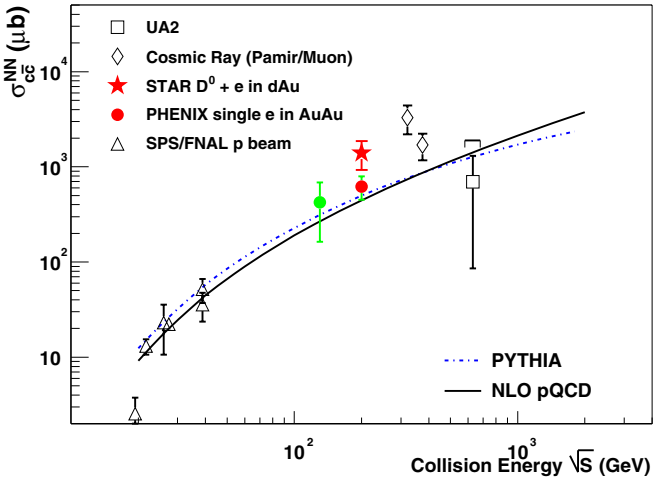


**Fig. 6.** Total $c\bar{c}$ cross section per binary collision vs. the collision energy $\sqrt{s_{NN}}$

Au+Au and pp distributions at $\sqrt{s_{NN}} = 200$ GeV. This difference is already apparent at $p_{\rm T} \simeq 2$ GeV/$c$, where statistics is still high, and can be due to interactions between heavy-quarks and the medium. The dead cone effect would reduce the amount of energy lost by heavy quarks in the medium [11] making the suppression at high-$p_{\rm T}$ smaller than the one for light-quark hadrons. However, this effect should be more evident at $p_{\rm T} \sim$ 5–10 GeV/$c$ and hence not yet accessible given the currently available statistics in central Au+Au collisions.

STAR has measured open charm in d+Au collisions through the direct $D^0$ reconstruction, $D^0(\bar{D^0}) \rightarrow K^{\mp}\pi^{\pm}$, as well as indirectly from non-photonic electrons at intermediate $p_{\rm T}$ (see [14] for details). By combining these measurements, the total charm cross-section per binary collision in d+Au collisions at $\sqrt{s_{NN}} = 200$ GeV is $\sigma_{c\bar{c}}^{NN} = 1.40 \pm 0.2_{stat} \pm 0.4_{sys}$ mb. The beam energy dependence of the cross section is presented in Fig. 6.

At $\sqrt{s_{NN}} = 200$ GeV both PYTHIA and NLO pQCD calculations [2,16] underpredict the total charm cross section by a factor $\sim$2–3. There are indications that a large charm cross section at $\sqrt{s_{NN}} \sim 300$ GeV is essential to explain cosmic ray data [19].

### 4.2 Charm elliptic flow

It has been argued that the matter created in heavy-ion collisions at RHIC is sufficiently hot and dense that charm quarks might thermalize in the medium [12]. The most promising method to study this hypothesis is the measurement of charm elliptic flow. As shown earlier, electron production at large $p_{\rm T}$ is dominated by electrons from semi-leptonic decays of heavy flavor hadrons. Already at $p_{\rm T} > 2$ GeV/$c$ the emission direction of the D meson is strongly correlated with the direction of the decay electron. Figure 7 shows the $\cos(\phi_{\rm electron} - \phi_{\rm D})$ distribution versus the electron $p_{\rm T}$ from simulated D-meson events. Consequently, the measurement of non-photonic electron

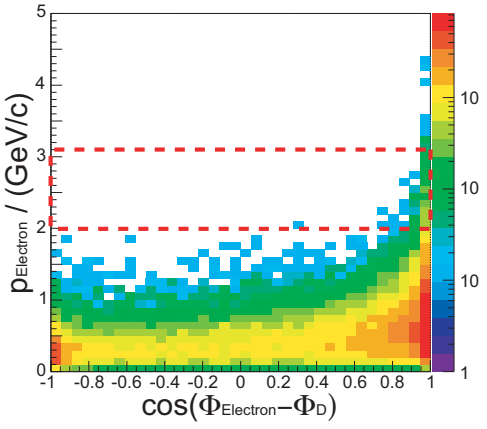


**Fig. 7.** Correlation between the electron momentum and the azimuthal angle difference between the D meson and the decay electron

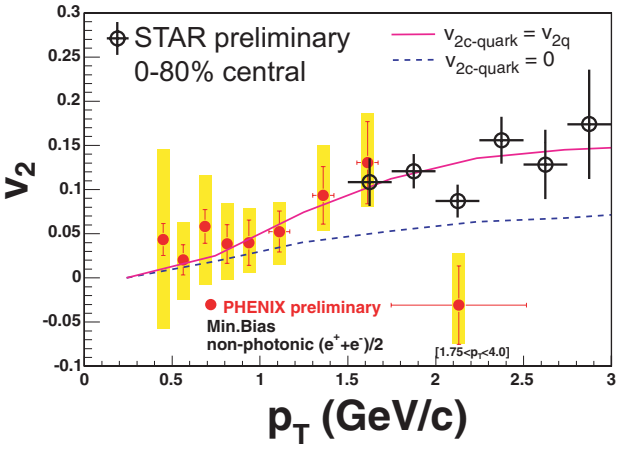


**Fig. 8.** $v_2$ from non-photonic $e^{\pm}$ vs. transverse momentum in Au+Au collisions at $\sqrt{s_{NN}} = 200$ GeV. The solid circles show preliminary results from the PHENIX experiment [23]

elliptic flow ($v_2$) in this $p_{\rm T}$ range reflects directly the flow of D mesons. The dashed lines in Fig. 7 depict the momentum range used in this analysis. The elliptic flow analysis in 200 GeV Au+Au collisions used the data recorded in 2001. During this run only a very small fraction of the STAR calorimeter was installed. We therefore used only the d$E$/d$x$ information from the TPC to select electrons. Before we correlate the electron azimuthal angle with the reaction plane, background electrons are removed using the methods described above. With detailed simulations of the STAR detector and using the $\pi^0$ distributions from [20] we estimate that this background subtraction method removes about 50 % of all photonic electrons.

The azimuth angle $\phi$ of the remaining $e^{\pm}$ is then correlated with the reaction-plane angle $\psi_{RP}$ (see [21] for details about reaction plane determination) and the $\cos\left(2[\phi - \psi_{RP}]\right)$ distribution is built. In the $p_{\rm T}$ interval 2–3 GeV/$c$ we estimate that the electron sample is composed of 63 % of electrons from D mesons and 37 % from remaining photonic sources (after the background subtraction). In order to correct for the remaining 37% $e^{\pm}$ background from photonic sources, we again use the $\pi^0$ spectrum from [20] onto which we impose elliptic flow according to [22] ($v_2^{\rm max} = 17\,\%$). Passing the resulting azimuthal anisotropy $\pi^0$ distribution through our detector simulation and analysis code we obtain a $\cos(2[\phi - \psi_{RP}])$ distribution for the remaining background. Subtracting this distribution from the uncorrected one we obtain the $\cos\left(2[\phi - \psi_{RP}]\right)$ distribution for $e^{\pm}$ from D-meson decays. The $v_2$ value for electrons from D-meson decays can then be calculated using $v_2 = \langle\cos\left(2[\phi - \psi_{RP}]\right)\rangle / \psi_{RP}^{\rm res}$. Here, $\psi_{RP}^{\rm res} \approx 0.7$ is the reaction-plane resolution which is determined via the sub-event method described in [21]. The average elliptic flow for electrons from D-meson decays is $v_{2e^{\pm}} \approx 0.15 \pm 0.02$ (stat) in the momentum interval 2–3 GeV/$c$. Our preliminary estimate of systematic uncertainties originates from uncertainties in $v_{2\pi^0}$ and in the exact amount of photonic $e^{\pm}$ background, and adds up to $\sim 25\,\%$ (relative). Other sources of systematic uncertainties are still under investigation.

Figure 8 shows the STAR preliminary single electron elliptic flow measurement (open circles). The error bars reflect only statistical uncertainties. The solid circles correspond to preliminary results from the PHENIX experiment at lower momentum [23]. The result obtained by the STAR experiment smoothly extrapolates to the PHENIX measurement. The solid and dashed lines are calculations from the Quark Coalescence Model [24] for two extreme cases. The solid line shows the expectations from a quark coalescence model with thermalized and flowing $c$ quarks and the dashed line shows the prediction for the case where $c$ quarks are not thermalized and do not flow. Despite the fact that the error bars are still large, the data points seem to favor the prediction from the quark coalescence model under the assumptions of a partonic stage with thermalized and strongly flowing $c$ quarks: $v_{2c} = v_{2{\rm light-quarks}}$. The systematic uncertainties still need to be evaluated in more detail and non-flow effects are still not estimated.

## 5 Summary

The transverse momentum distributions of non-photonic electrons have been measured at STAR in pp and d+Au collisions. By combining the electron measurements with the direct reconstruction of D mesons it was possible to obtain the total charm cross section in d+Au collisions. Both Pythia and NLO pQCD calculations underpredict the charm cross section at RHIC energies. In-medium modifications can be studied by comparing charm production in pp with d+Au and Au+Au collisions. There is no evidence for any nuclear modification in d+Au collisions at $\sqrt{s_{NN}} = 200$ GeV. The very limited high-$p_T$ statistics in central Au+Au collisions measured by the PHENIX experiment, at the present, does not allow to draw any conclusion on medium modifications. On the other hand, preliminary elliptic flow measurements for non-photonic electrons indicate a strong interaction between the heavy quarks and the medium. STAR and PHENIX $v_2$ results for

electrons, when compared to Quark Coalescence Models, suggest that $c$ quarks interact with thermalized partonic matter and appear to have about the same flow as light quarks. The year 2004 Au+Au data will allow a spectrum and elliptic flow measurements of non-photonic electrons at high-$p_T$ with increased statistics and will address these subjects more precisely.

*Acknowledgements.* We thank the RHIC Operations Group and RCF at BNL, and the NERSC Center at LBNL for their support. This work was supported in part by the HENP Divisions of the Office of Science of the U.S. DOE; the U.S. NSF; the BMBF of Germany; IN2P3, RA, RPL, and EMN of France; EPSRC of the United Kingdom; FAPESP of Brazil; the Russian Ministry of Science and Technology; the Ministry of Education and the NNSFC of China; Grant Agency of the Czech Republic, FOM and UU of the Netherlands, DAE, DST, and CSIR of the Government of India; Swiss NSF; the Polish State Committee for Scientific Research; and the STAA of Russia.

## References

1. S. Frixione et al., Adv. Ser. Direct. High Energy Phys. **15**, 609 (1998) [hep-ph/9702287]
2. R. Vogt, hep-ph/0203151
3. B. Muller, X.N. Wang, Phys. Rev. Lett. **68**, 2437 (1992)
4. J.P. Blaziot, Nucl. Phys. A **661**, 3c (1998)
5. P.M. Jacobs, X.-N. Wang, hep-ph/0405125
6. T.S. Ullrich, Nucl. Phys. A **715**, 399c (2003)
7. P.F. Kolb, U. Heinz, nucl-th/0305084
8. C. Adler et al. (STAR Coll.), Phys. Rev. Lett. **89**, 292301 (2002)
9. C. Adler et al. (STAR Coll.), Phys. Rev. Lett. **90**, 082302 (2003)
10. C. Adler et al. (STAR Coll.), Phys. Rev. Lett. **91**, 072304 (2003)
11. Y.L. Dokshitzer, D.E. Kharzeev, Phys. Lett. B **519**, 199 (2001)
12. X. Dong et al., Phys. Lett. B **597**, 328 (2004)
13. M.C. Abreu et al. (NA50 Coll.), Phys. Lett. B **477**, 28 (2000)
14. J. Adams et al. (STAR Coll.), Phys. Rev. Lett. **94**, 062301 (2005)
15. The Relativistic Heavy-Ion Collider Project: RHIC and its detectors, Nucl. Instrum. and Meth. A **499** (2003)
16. T. Sjöstrand et al., Comp. Phys. Commun. **135**, 238 (2001) [hep-ph/0010017]
17. X.-N. Wang, M. Gyulassy, Phys. Rev. D **44**, 3501 (1991)
18. S.S. Adler et al. (PHENIX Coll.), nucl-ex/0409028
19. I.V. Rakobolskaya et al., Nucl. Phys. B **112**, 353c (2003)
20. S.S. Adler et al., Phys. Rev. Lett. **91**, 0702301 (2003)
21. C. Adler et al. (STAR Coll.), Phys. Rev. C **66**, 034904 (2004)
22. K. Schweda, J. Phys. G **30**, S693 (2004)
23. M. Kaneta et al. (PHENIX Coll.), J. Phys. G **30**, S1217 (2004)
24. V. Greco, C.M. Ko, nucl-th/0405040